One-Level Diagnostic Modeling of Mesoscale Surface Winds in Complex Terrain. Part I: Comparison with Three-Dimensional Modeling in Israel

P. ALPERT* AND B. GETENIO

Department of Geophysics and Planetary Sciences, Tel Aviv University, Ramat Aviv, Israel

(Manuscript received 6 February 1987, in final form 28 January 1988)

ABSTRACT

A one-level sigma-coordinate model originally developed by Danard and modified by Mass and Dempsey and Alpert et al., is applied to the study of surface flow over an averaged summer diurnal cycle in Israel. The detailed flow features are compared to three-dimensional modeling studies and to dense surface wind observations.

The winds at a height of 10 m from the one-level model were found comparable to those obtained by three-dimensional simulations, and in some cases the one-level model predicted observed surface flow features that were not simulated by the three-dimensional simulations, probably because of the finer horizontal grid resolution in the one-level model. The two models had similar deficiencies in diagnosing observed flow features in many cases. A severe drawback of the one-level model is the inability to advance the sea-breeze front (SBF) over a ridge crest correctly. Based upon an earlier vertical cross-sectional study by Alpert et al., an explanation for this discrepancy is suggested.

In a detailed, high-resolution analysis of the summer mesoscale flow, the surface horizontal winds from the one-level high-resolution model and the three-dimensional model are compared to the relatively dense network of wind observations in Israel every three hours, for an averaged diurnal cycle. Several features of the surface flow are revealed and illustrated, including

(i) Flow convergence in the evening near the coast;

(ii) A convergence line south of Lake Kinneret (Sea of Galilee) that forms in the morning, moves southward along the Jordan Rift Valley, and finally merges with the SBF in the afternoon;

(iii) Relatively strong nocturnal flow at the southern Mediterranean coast of Israel, possibly due to the concave shoreline there.

These, as well as many other observed flow features, are simulated by both the one-level model and the three-dimensional model, though the one-level model required only modest computer resources. Hence, this study illustrates that the trade-off between horizontal resolution and explicit vertical resolution may be most beneficial, at least when topographic and surface forcing dominate.

1. Introduction

The enormous computing time required by three-dimensional (3-D) mesoscale models to calculate detailed surface winds has encouraged the development of several simpler models that diagnose surface winds over complex terrain. The simpler models can be separated into three classes according to their physical assumptions: 1) mass conservation models, 2) one-layer primitive equation models that assume a well-mixed boundary layer, and 3) one-level models that solve the momentum and energy equations at the surface. The advantages and disadvantages of each of these model types were summarized, for example, by Mass and

Dempsey (1985; here denoted as MD). The mass conservation models are, in general, based only upon the equation of continuity and therefore depend strongly on the quality and quantity of the input data (e.g., see Dickerson 1978). The other two classes of simple models solve the energy and momentum conservation equations and include diabatic heating, nonlinear advection, friction, Coriolis and pressure gradient forces. They are not necessarily dependent on surface input data and may be initialized without any surface data at all. The mixed-layer models solve the primitive equations, including the continuity equation, within an assumed well-mixed boundary layer. In contrast, the one-level models replace the continuity equation with a parametrization of a "layer of topographic influence," within which the temperature lapse rate is assumed independent of height but can vary horizontally and temporally. The lapse rate is recalculated at each time step according to the updated surface temperature. Consequently, this model can be operated *diurnally*, as in the present study. The mixed layer

---

* Visiting the Department of Meteorology, Reading University, England.

Corresponding author address: Pinhas Alpert, Dept. of Geophysics and Planetary Sciences, Tel-Aviv University, Tel-Aviv 69978, Israel.

model was introduced by Lavoie (1972) and further investigated for real-data forecasting by, e.g., Keyser and Anthes (1977). The one-level model was first developed by Danard (1977) and recently improved by Mass and Dempsey (1985). The MD version with some minor modifications was employed in the present study.

Let us first briefly summarize the potential advantages of a one-level model over a 3-D model. There are still serious problems in initializing 3-D mesoscale models with spatially or temporally varying synoptic-scale conditions. It will be shown later (as illustrated by MD as well) that the one-level model can be easily used even with a spatially varying large-scale pressure gradient. Also, when sufficient mesoscale data for initialization and boundary specification are not available, the 3-D models may lose their advantage because for satisfactory 3-D simulations—particularly over complex terrain—such data appear to be essential. In addition, there is a great demand for simplified models that could be operated with modest computer resources at local forecast offices or even at forecasting centers. The 3-D models require computer resources that are in excess of what is commonly available at such locations. A natural question that thus arises regarding one-level models is whether the saving in computing time, though considerable, can justify the major physical simplications employed by these models. The answer to this question is affirmative if these simplified models can compete well with 3-D models and in certain cases can solve problems that 3-D models cannot.

The purpose of this study is to compare, for the first time, the abilities of 3-D models and a one-level model of the Danard–MD type to diagnose the surface winds during a typical summer day in Israel. This comparison is done for a full diurnal cycle along with the analysis of a dense net of averaged surface wind observations. A similar study for a mixed-layer model was performed by Anthes et al. (1980). A companion to this study (Alpert et al. 1988) examines the applicability of the model to real data forecasting.

Alpert and Eppel (1985), using an index for mesoscale activity based on surface-wind variability, found that the mesoscale forcing in Israel is strong. This makes Israel an ideal location for studying mesoscale flows, and consequently, a relatively high number of 2-D as well as 3-D summer simulations have been performed in Israel. In summer, the daytime circulation is dominated by the Mediterranean sea breeze and vigorous upslope winds, while at night a shallow land breeze develops, which is enhanced by slope flows down the western slopes. The complex flow for a 2-D vertical cross section in northern Israel, latitude of $\sim$33°N, from the Eastern Mediterranean past Lake Kinneret in the Jordan Valley was simulated by Alpert et al. (1982). Other 2-D simulations in Israel were reported by Neumann and Mahrer (1971), Doron and Neumann (1977), Segal et al. (1982a) and Alpert et al. (1985), while 3-D simulations were performed by

Anthes and Warner (1978), Segal et al. (1982b), Mahrer and Segal (1984), Segal et al. (1985) and Mahrer et al. (1985). The three-way coincidence that occurs in Israel, i.e., high mesoscale activity, a multitude of 2-D and 3-D simulations, and a dense net of observations, provides a unique opportunity for a careful comparison of the one-level model performance with a detailed description of a typical evolution of summer mesoscale flow in Israel. The results from all the models listed above will be used for model comparisons.

The modified model is described in section 2, while the simulations are presented in section 3.

2. The model

a. The model equations

The two basic equations we solve are the horizontal momentum conservation relation and the thermodynamic energy equation on a sigma-surface ($\sigma = 1$). Following MD, we parametrize the effects of topographic and surface forcing by assuming the existence of a "layer of topographic influence" of depth H above the surface ($H = 1$ km in the following experiments), and we assume that we know the synoptic-scale height (Z_R) and temperature (T_R) fields on a reference pressure-level, 700 mb. The "free atmosphere" lapse rate, i.e., between Z_H and Z_R, was derived from the nearby soundings and was assumed independent of time, while the lapse rate between the surface and Z_H was assumed to be independent of height but was recalculated at each grid point and at every time step according to the new surface temperature from the thermodynamic energy equation. Integrating the hydrostatic relation from the surface to the height of topographic influence and from Z_H to Z_R yields an expression for $\ln p_s$ in terms of the surface temperature, which then closes the model equations.

The final equations the model solves are

$$\frac{\partial \mathbf{V}_s}{\partial t} = -\mathbf{V}_s \cdot \nabla_\sigma \mathbf{V}_s - f\mathbf{k} \times \mathbf{V}_s + \mathbf{F} + K_m \nabla_\sigma^2 \mathbf{V}_s$$

$$- g\{(e_1 - H/T_H)\nabla_\sigma T_s - [e_1 + (e_2/(\gamma T_R))]$$

$$\times (T_H - T_R)]\nabla_\sigma T_R + (\gamma e_1 - e_2 + 1)\nabla_\sigma z_s$$

$$+ (e_2 - \gamma e_1)\nabla_\sigma Z_R\} \quad (1)$$

$$\frac{\partial T_s}{\partial t} = -\mathbf{V}_s \cdot \nabla_\sigma T_s - (A_2/A_1)\mathbf{V}_s \cdot \nabla_\sigma T_H$$

$$- (A_3/A_1)\mathbf{V}_s \cdot \nabla_\sigma T_R + Q/(A_1 C_p) + K_T A_1^{-1} \nabla^2 T_s. \quad (2)$$

These follow Eqs. (1), (14) and (11) in MD, where the derivation can be found. A list of symbols is given in the Appendix.

The notion of "layer of topographic influence," H, needs some clarification (personal communication, D. Dempsey). The parameter H appears in the equations for the following reasons. In an effort to develop computationally efficient, mesoscale surface wind models
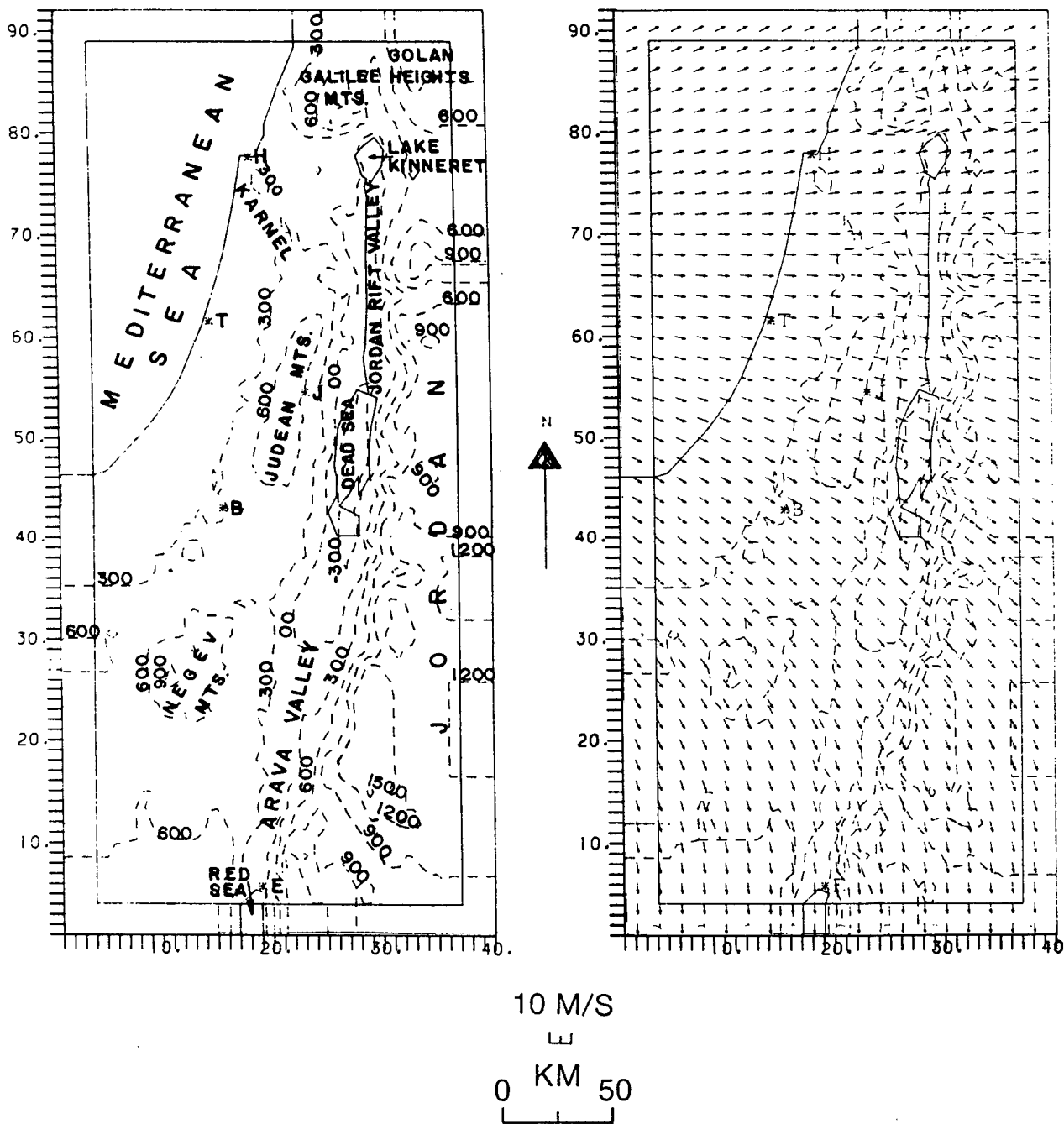
FIG. 1. (a) The model domain and its main geographical features. The topography is illustrated by the 300 m contours (dashed lines). The points H, T, J, B, and E denote the towns of Haifa, Tel Aviv, Jerusalem, Beer-Sheva, and Eilat, respectively. (b) The large-scale wind input corresponding to the average July wind.

for use in complex terrain, Danard and subsequently MD chose try to solve the equations of motion in sigma-coordinates at one level only, the surface, subject to the hydrostatic assumption. They found that they could not use the continuity equation explicitly under the constraints of their objectives, and consequently, they had one more dependent variable than they had equations to relate variables. This required that they make some additional assumptions about the relations between their dependent variables, and they saw that they could close their equations by making assumptions about the temperature profile if the temperature and pressure are independently known at some level. The simplest and most convenient way to handle this is to assume that temperatures and pressures at a standard pressure level are "known" from observations (or

specified in the absence of observations) and that sur-
face effects on the temperature vanish at some level.
This level, embodied in the parameter H, is a new vari-
able and additional assumptions must be made about
it. Danard decided that it would be a boundary layer
depth and treated it as such, even though it arose as a
consequence of the lack of a continuity equation and
was therefore not necessarily connected to boundary
layer processes at all. Mass and Dempsey (1985) treated
it as a parameter that, together with their assumptions
about the temperature profile, allowed their model to
mimic qualitatively the behavior of inviscid, adiabatic
flow past sufficiently high, 3-D mesoscale topography
as if it were actually satisfying the continuity equation
in addition to the other members of the primitive
equation set. Hence, H was initially a parameter as-
sociated with the parametrization of the dynamic effects
of mesoscale flow past 3-D topography. It did not nec-
essarily have anything to do with boundary layer pro-
cesses. But MD used H in their treatment of surface
heating and cooling as well as surface friction. By
choosing H as a representative value of the boundary
layer depth as well, they have parametrized boundary
layer processes with less flexibility than they might have
had if they had hypothesized a *separate* boundary layer
depth and developed an equation for it or otherwise
specified it. Such an approach would separate the
purely dynamical effects of topography from surface
effects. In the present work we have not attempted such
an approach but instead have followed the MD para-
metrization.

b. Numerical aspects

For the initialization procedure and the boundary
conditions, as well as most of the numerical schemes
(except those referenced later explicitly), the reader is
referred to MD. However, there are some modifications
that were found useful in the forthcoming experiments.
The modifications include

(i) The drag coefficient C_D in the parametrization
of the surface friction was calculated according to

$$C_D = [k/\ln(z/z_0)]^2$$

where $k \sim 0.4$ is Von Karman's constant, $z = 10$ m
is the standard anemometer level, and z_0, the roughness
length, was specified to be 10^{-1} m over land and 10^{-4}
m over sea or lake. Hence, C_D values are $0.75 \cdot 10^{-2}$
and $1.2 \cdot 10^{-3}$ over land and sea, respectively. Mass and
Dempsey (1985) adopted the constant values of $2 \cdot 10^{-2}$
and $1.4 \cdot 10^{-3}$, respectively. Although this formula is
strictly valid only for a neutrally stratified PBL, it was
used for the crude estimation of effects due to possible
changes of the roughness length.

The frictional force F is proportional to C_D through

$$F = -C_D V_s |V_s|/H.$$

This assumes a linear stress profile through the layer
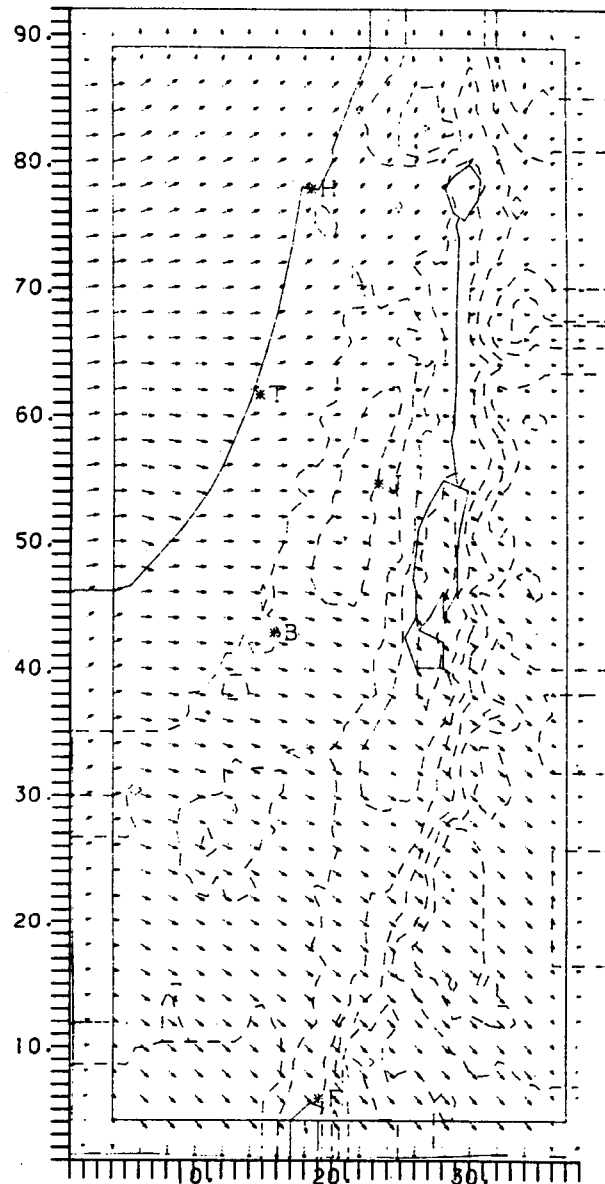of depth H, and corrections for different stabilities were

FIG. 2. The Ekman solution for the surface winds—
first stage of integration (see text).

incorporated following MD (see their appendix A, p.
1225). Another assumption included in the derivation
of F is that the depth of the layer of topographic influ-
ence characterizes the depth of the planetary boundary
layer.

(ii) The temperature and geopotential heights at 700
mb are interpolated from the nearby radiosondes to
the model grid through the Cressman analysis (e.g., see
Haltiner and Williams 1980, p. 357). The optimum
radius of influence is determined by the formula sug-
gested by Goodin et al. (1979). Here the reference level
was chosen at 700 mb rather than 850 mb since the
Eilat 850 mb sounding was suspected to be strongly
influenced by the high terrain in the southern region
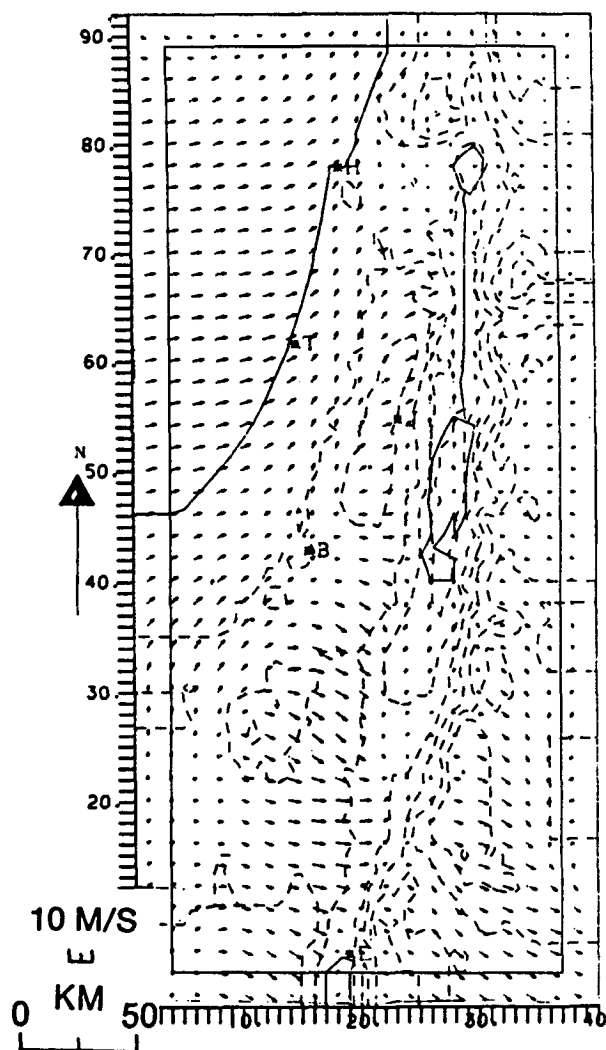(see Fig. 1a).

10 M/S

0 KM 50

FIG. 3. The steady-state solution—second stage of integration.

(iii) To reduce possible disturbances near the boundaries, the gradients of the topography (z_s), and of the reference-level geopotential (Z_R) and temperature (T_R), were assumed zero at the four grid points close to the boundaries. Hence, the flow at the boundaries may be distorted to some extent, and the pertinent region is therefore indicated in the following figures. This method has reduced the boundary disturbances but not eliminated them completely, as discussed later.

In the following experiments the equations were solved over a 92 × 40 mesh with a constant grid-interval of $\Delta x = \Delta y = 5$ km. The time interval was 90 sec. The values of the turbulent diffusivities for momentum and temperature were chosen equal, $K_m = K_T = 2 \times 10^4$ m s^{-1}.

As in MD, the horizontal temperature diffusion was performed along horizontal Z-surfaces rather than along sigma-surfaces because calculation of the horizontal diffusion over the sloped sigma-surfaces may lead to excessive smoothing over topography, as was illustrated by Alpert and Neumann (1984). This enhanced smoothing along the sigma-surfaces has resulted in diminishing the vertical velocities in a sea-breeze front. Of course, the temperature diffusion on a constant σ-surface represents spurious diabatic forcing on a constant Z-surface as long as the σ-surfaces are not horizontal.

3. Model simulations and comparison with 3-D modeling results

a. Initialization

The model domain includes Israel and the surroundings from 29° to ~33.5°N and from ~33.5° to 36°E. The area consists of the Mediterranean Sea to the northwest; Lake Kinneret (at −200 m MSL) and the Dead Sea (~−400 m MSL), which are both sur-

TABLE 1. Some characteristics of the model simulations cited in this study.

Model reference	Abbreviated reference in text	Domain (Part of Israel encompassed)	Grid resolution $(\Delta x, \Delta y)$ (km)	Synoptic wind at ~700 mb (m s^{-1})	Height of surface simulation (m, AGL)	Diabatic heating
Present study	—	North + South	(5, 5)	Variable: 240°/05 north to 360°/ 05 south	10	Sinusoidally
Segal et al. (1982b)	S82	North	(5, 5)	250/06	10	Explicit calculation of surface temperature, sensible heat flux, radiation, etc.
Segal et al. (1985)*	S85	South	(5, 10)	250/06	5	
Mahrer and Segal (1984)	MS	North + South	(5, 10)	250/06	5	
Anthens and Warner (1978)	AW	Central	(7.3, 7.3)	calm	~290	Sinousidally

* This simulation is identical to MS except that it includes only the southern region of Israel.
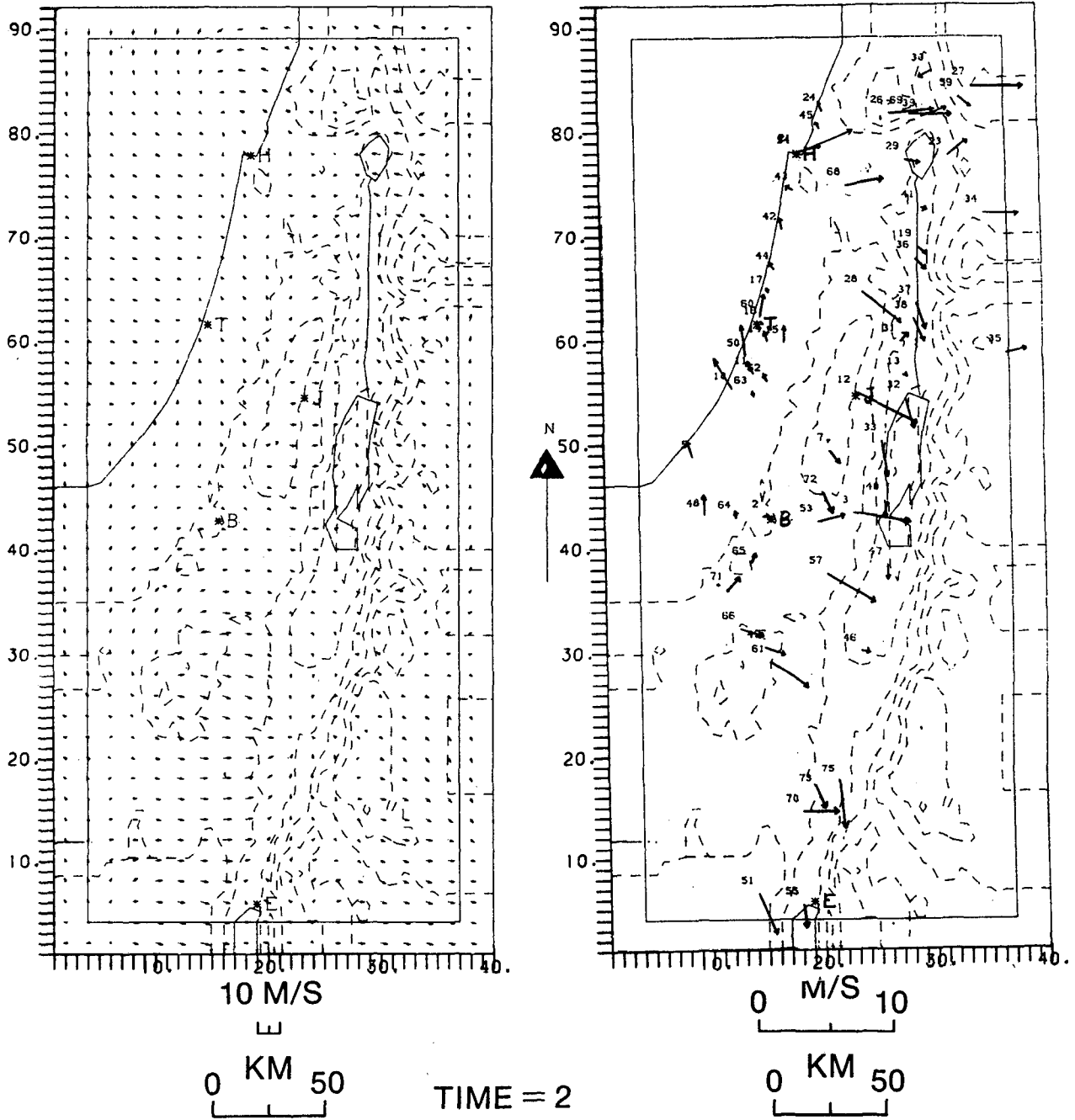
FIG. 4. (a) One-level model surface winds for the average July conditions at 0200 LST (0000 UTC).
(b) July averaged observed winds at 0200 LST.

rounded by high mountains, from east and west; and the northern corner of the Red Sea on the southern boundary of the region (see Fig. 1a). The lakes are located in the Jordan Rift Valley (hereafter JRV) with a north to south mountain line in the west running from the Galilee through Judea to the Central Negev. To the east of the JRV a second mountain line is approximately oriented from north to south. The mountains change from the Golan Heights in the north, through the elevated plateau of Jordan, exceeding 1500 m to

the southeast of the Dead Sea. The topography is illustrated by the 300 m contours (dashed lines) in Fig. 1a and subsequent figures. Figure 1b presents the large-scale input geostrophic wind,[1] which was assumed to vary linearly from 240°/05 m s^{-1} in northern Israel to

---

[1] Note that for greater clarity of presentation the vector wind plots here and on the subsequent surface wind simulations show every other vector rather than all the vectors in the domain.

HOUR : 2.00 LST   10 M/S
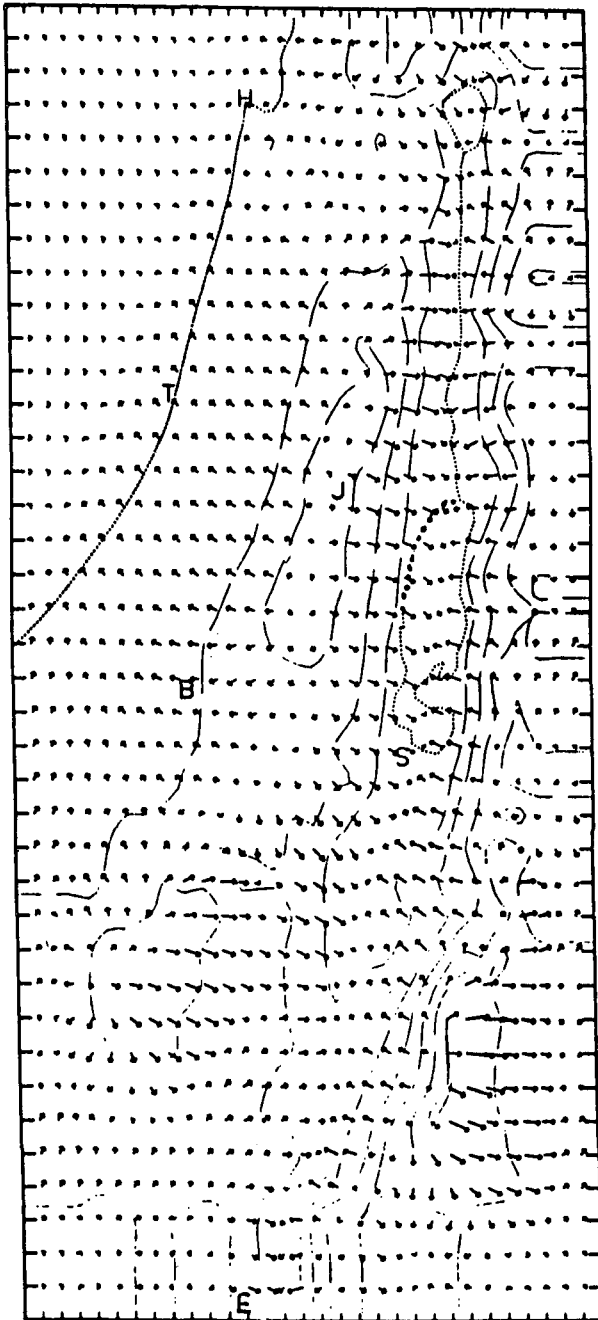HORIZONTAL VELOCITY AT 5.M

FIG. 4c. 3-D model results for a typical summer day
at 0200 LST, from MS.

July temperature at 700 mb, Bet Dagan. The free at-
mosphere lapse rate was taken to be 6.5°C km^{-1} fol-
lowing the July averaged value below the typical sum-
mer inversion (e.g., see Alpert et al. 1982).

The model was first solved iteratively to get the bal-
ance for the large-scale pressure-gradient force, surface
friction and the Coriolis force. The result corresponds
to an Ekman type solution—but for nonhomogeneous
conditions and a very different stress parametrization—
and is presented in Fig. 2. As expected, surface winds
are weaker relative to the large-scale flow, especially
above land, and are directed toward the lower pressure.
The flow in Fig. 2 does not include the temperature
advection along sloped surfaces, which in the stratified
model atmosphere allows the model to parametrize
the pressure perturbations normally associated with the
dynamic effects of topography.

The second integration step was to include all other
terms except the diabatic heating. This means that ad-
vection, diffusion and pressure-gradient forces arising
from interaction with the topography were all included
at this stage. Since the diabatic forcing was not yet in
the model, it could be integrated until a steady state
was reached (see Fig. 3). About 300 time steps were
necessary to reach this steady-state solution.[2] Figure 3
shows the dynamical effect of the mountains, which
channel the flow in the JRV and deflect the flow around
the high mountains, in contrast to the flow in Fig. 2.

b. The diabatic forcing

Following MD (their Fig. 2) the diabatic forcing was
assumed to vary sinusoidally from pre-sunrise (ap-
proximately 0230 UTC or 0430 LST) to post-sunset
(~1700 UTC or 1900 LST) while being constant (neg-
ative) during the night. At the exact sunrise and sunset
the diabatic heating is put to zero. The maximum am-
plitude of heating by day was estimated to be 2°C h^{-1}
and by night −0.5°C h^{-1}. The corresponding values
over water were 0.17° and −0.08°C h^{-1} (which are
2°C/12 h and −1°C/12 h, respectively). The procedure
for determining these values was described by MD (see
their p. 1214 and appendix D).

c. Method of comparison

As the model reached the steady-state solution, the
diabatic forcing was introduced starting at sunrise
(where it was assumed zero) and then run for over 24
hours to follow a full diurnal cycle. In each of the fol-
lowing figures we will present our model results every
three hours starting at 0200 LST (part a in Figs. 4–
11), along with July averaged observed wind vectors
for more than 70 stations (Part b in Figs. 4–11), and
any available 3-D simulations for the same hour (part
c in Figs. 4–10 and part d in Figs. 7 and 9). All figures

360°/05 m s^{-1} in the south, corresponding to the av-
erage July wind at the reference level Z_R (700 mb).
They were estimated from the average Bet Dagan (sta-
tion No. 40179) sounding and the few pilot balloons
available in the region.

The temperature at the reference level was assumed
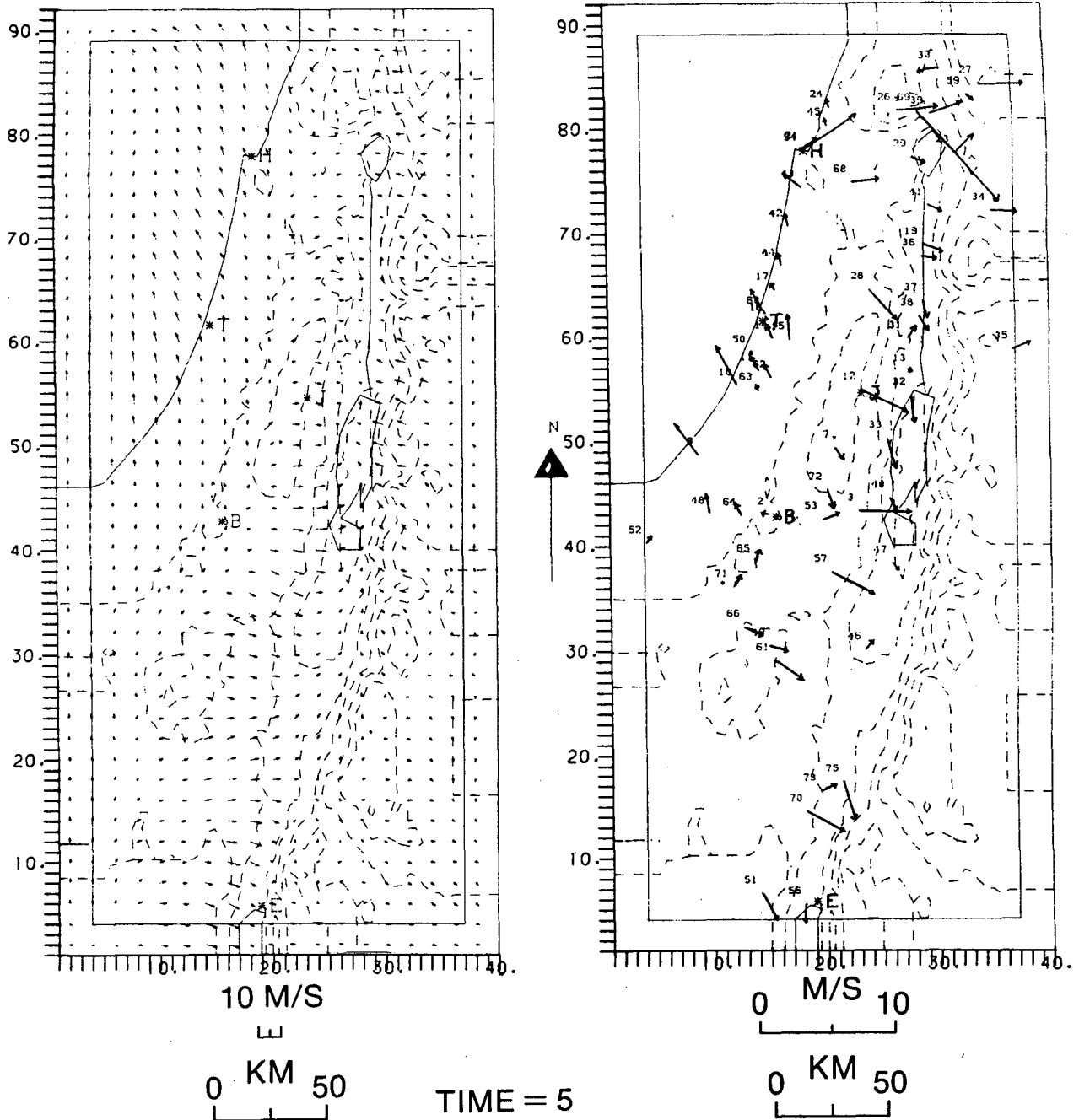constant, $T_R = 282.14$ K, corresponding to the average

FIG. 5. (a, b) As in Fig. 4a, b but at 0500 LST.

presented are for average summer conditions. We have preferred to compare the model results directly with averaged observed wind data rather than with the objective (Doron 1979), or the subjective (Skibin and Hod 1979) analyses of averaged summer wind fields for the following reasons:

(i) We have included, in addition to the stations that were used by Doron (1979) and Skibin and Hod (1979),

an additional 27 stations provided by the Israel Meteorological Service (IMS).

(ii) In doing a careful comparison of model results with observations, one should be aware of the very different resolution of surface observations in various regions. For example, in the Negev desert region there are only a few stations over a relatively large domain, while at the coastal plain of Israel there are many stations over a much smaller domain (see Fig. 4b). The
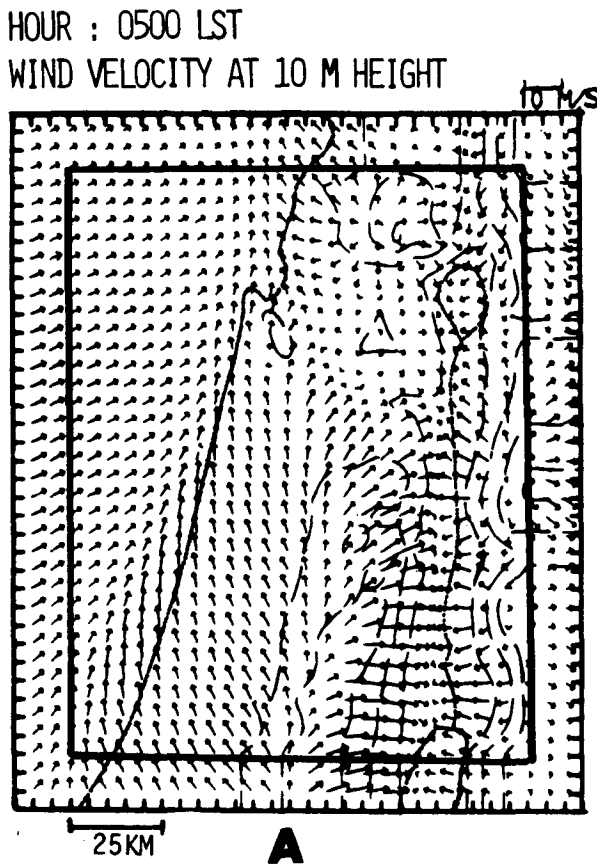
HOUR : 0500 LST
WIND VELOCITY AT 10 M HEIGHT

FIG. 5c. As in Fig. 4c but at 0500 LST and from S82.

average distance between two observation points is ~31 km over the full model domain, while this distance is only about 12 km over a triangle that covers the coastal plain of Israel. Therefore, in any comparison between two models or between model and observations, we prefer to discuss the flow features evident in the direct observations, rather than in a derived analysis.

In parts c and d of Figs. 4–11, we have presented the 3-D model simulations that were available for average summer conditions, although there were some small differences in the input conditions between the 3-D model runs as well as between the 3-D and 2-D model runs. Their effect was judged to be unimportant based upon the experience of the authors in studying the summer flow in Israel. Table 1 presents some of the 3-D model specifications, which will be of interest in comparing the modeling results.

d. Diurnal simulations and observations

(i) *0200 LST:* The surface nocturnal flow for 0200 LST for average July conditions is presented in Figs. 4a to 4c, where Fig. 4a presents the one-level, 2-D model, Fig. 4b the averaged observations, and Fig. 4c

the 3-D model results from MS. Both numerical models succeeded in producing most of the flow features. Some of these include the southeasterly land breeze on the coastal plain supported by nocturnal drainage along the western slopes of the first line of mountains (except Haifa point H), the relatively strong northwesterly winds on the lee side of this mountain line, and the northwesterly winds on the western slope to the JRV. However, there are some observational features that are not reproduced by the models: the westerly flow over the Golan Heights as well as over the other mountains in Jordan, the northerly wind on the northern coast of the Red Sea (at Eilat, point E), the weak northerly wind to the south of the Dead Sea, and the nearly northerlies in the western JRV. The discrepancies between the models and the observations are nearly the same for both the 2-D and the 3-D models. While the first two discrepancies could be associated with the proximity of the boundary, the latter two might be the result of inadequate resolution. Unfortunately, there is no observational basis for deciding which model is correct in some regions where there are major differences between the models, as for example the direction of the winds south of Beer-Sheva (station B). They are easterlies in the 3-D simulation but weak westerlies in the 2-D simulation.

(ii) *0500 LST:* The model results versus observations do not change appreciably three hours later at around sunrise (~0500 LST), as illustrated in Figs. 5a to 5c. The 3-D model results for this hour are from Segal et al. (1982b; hereafter referred to as S82), where only the northern region was simulated but with a higher horizontal resolution of $\Delta x = \Delta y = 5$ km (see Table 1). It should be pointed out the 3-D model simulation with the higher horizontal resolution for the full domain has not yet been performed due to limitations on computer resources. Therefore, the one-level model results are the only model simulation with 5-km grid resolution over the full domain. This technical point might make the one-level model more realistic by allowing it to include both a larger domain and high *horizontal* resolution. But this becomes possible only because the one-level model very simply parametrizes the interactions between the surface flow and the atmosphere above. The trade-off between horizontal resolution and explicit vertical resolution may not always be beneficial. The trade-off does seem worthwhile, at least in the simulations presented here.

Returning to Fig. 5a, the nocturnal flow, simulated by the one-level model, in particular into the JRV from both slopes, is somewhat stronger than at 0200 LST, but evidence for that is not available from observations. Interesting to note is the fact that the convergence line over the Mediterranean Sea, about 15–25 km from the northern shore, is supported by the 3-D simulation (Fig. 5c). Alpert et al. (1982) have suggested this convergence line along the shore to be responsible for the early morning stratus line typical for the summer morning
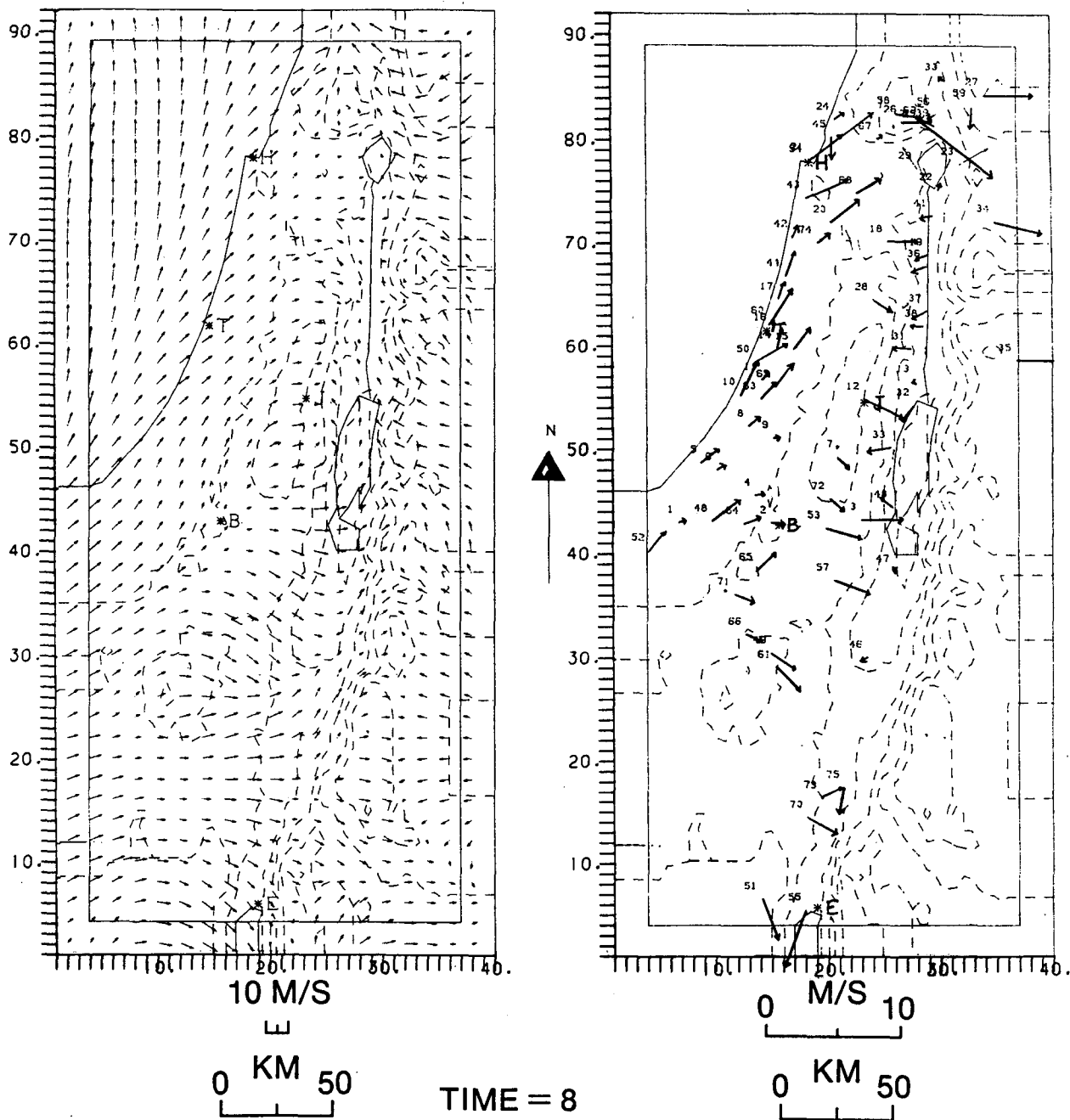
FIG. 6. (a, b) As in Fig. 4a, b but for 0800 LST.

offshore. The flow features in the model and the observations at 0500 LST are quite similar to these at 0200 LST. The one-level, 2-D model and the 3-D model again exhibit similar model discrepancies.

Another feature of the 0500 LST flow as well as that of 0200 LST is the stronger southeasterly winds at the southern as compared to the northern coast, i.e., at about 20–60 km south of Tel Aviv compared to the southeasterlies north of Tel Aviv (see Figs. 5b and 4b). We suggest that this stronger land-breeze/katabatic flow in the south is associated with convergence along the

concave shoreline there. The effect of a convex shore upon land and sea breezes has already been pointed out by Neumann (1951) and Neumann and Mahrer (1974) but we are not aware of observations that seem to indicate directly this effect upon the land-breeze. There are some indications of enhanced flow in the model simulations as well (see Figs. 4a, 4c and 5a), but they are not as strong as in the observations.

(iii) *0800 LST:* Figures 6a to 6c present the flow patterns at 0800 LST, about three hours past sunrise during the start-up of daytime thermal circulations.

HOUR : 0800

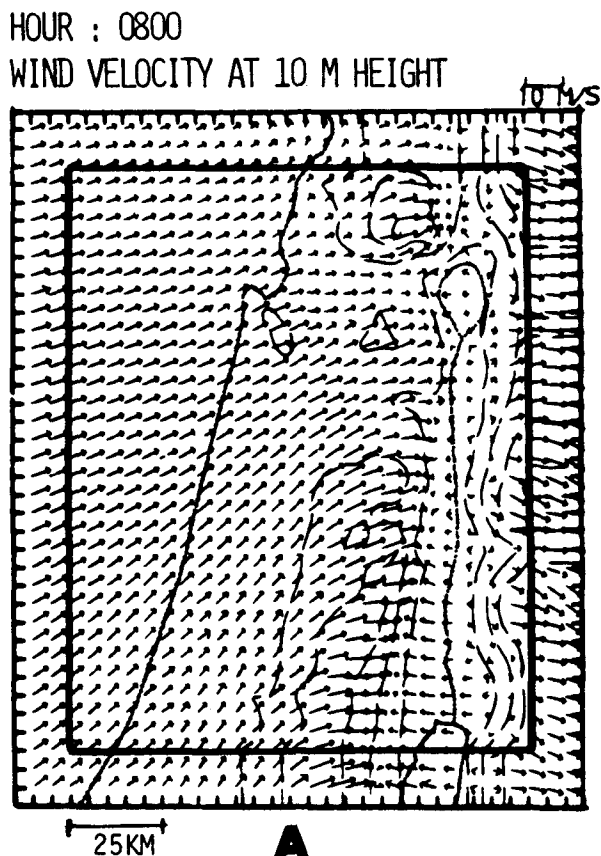WIND VELOCITY AT 10 M HEIGHT

FIG. 6c. As in Fig. 5c but for 0800 LST.

Along the coastal plain the winds have veered clockwise (see Haurwitz 1947), to become southwesterly. Over the central mountain tops the winds remain westerly to northwesterly in both models and observations. These westerlies hardly change during the day, probably due to the large-scale dominance over mesoscale surface forcing at high elevations. Along the western part of the southern JRV, thermally induced easterly upslope winds appear. These easterly upslope winds are weaker in the northern section of the JRV only in the model simulations, not in the observations.

Here again we do not have 3-D results for the southern section, but the few observations in the Negev are simulated well by the one-level model, except for the north-northeasterly wind at the Arava Valley and at Eilat (point E). The model predicts northwesterlies while Eilat observations indicate a northeasterly wind. This problem exists with the 3-D models as well, which are unable to predict the consistent northerly wind at that point. The models' poor performance at Eilat might be the result of either a lateral boundary disturbance or inadequate resolution (see the discussion by Segal et al. 1985, hereafter referred to as S85).

(iv) *1100 LST:* The simulated and observed flows are shown in Figs. 7a to 7d. Figure 7d presents the simulation results from Anthes and Warner (1978;

hereafter AW). Although there are some important differences[3] between AW (3-D) simulation and the other studies, e.g., the ~290 m altitude of the lowest sigma-surface, it will be shown that the major observed features are simulated. The coastal plain of Israel is dominated by the relatively strong northwesterlies, due primarily to the Mediterranean Sea breeze. The sea breeze is accompanied by the anabatic, thermally induced winds up the mountain slopes, which support the sea breeze on the western side of the central mountain line but oppose the sea breeze on the east (the lee side), forming a sharp SBF nearly along the crest of the mountains.

The southeasterlies all the way from the Sea of Galilee through the JRV to the Dead Sea and the Arava Valley clearly indicate the SBF location both in the model simulations (Figs. 7a, 7c, 7d) and in the observations (Fig. 7b). Although there are not enough observations to locate the SBF exactly, it seems that the front to the south of the Judean Mountains is a little retarded in the one-level simulation (Fig. 7a), and we shall return to this point later. The same is true of the AW simulations (Fig. 7d), but there it may be explained by the fact that the six hours of heating in AW end *prior* to 1100 LST, at around 1030 LST. Thus, Fig. 7d is better applied to ~1030 LST.

Strong convergence between the southern shore of the Sea of Galilee and the region 10–15 km to the south appears clearly both in the observations (northerly and southerly winds in the observations at sites 22 and 41 in Fig. 7b) and in the one-level simulation (Fig. 7a). The convergence, which to our knowledge has not previously been reported in observational or modeling studies, is probably the product of the local lake breeze, which opposes the southerly winds from the JRV. This, as well as the nearly southerlies that are observed in the JRV (Fig. 7b) are not as well simulated by the 3-D model (Fig. 7c) and it is probably the result of the poorer resolution in the north–south direction in the 3-D model ($\Delta y = 10$ km) compared to the one-level model ($\Delta y = 5$ km). The poorer resolution considerably diminishes the local sea-breeze effect of the Sea of Galilee. The success of the one-level model in this case illustrates its potential to simulate high-resolution surface winds over complex terrain.

Another problem that might be related to a boundary disturbance is the easterly winds along the eastern model domain to the east of Galilee and to the northeast of Eilat (Fig. 7a). The 3-D model results of Mahrer and Segal (1984) in Fig. 7c do not predict these winds but the 3-D model results of AW (Fig. 7d) do predict easterlies to the northeast of Eilat. This difference between the models' predictions might partly be explained by the topographical input; in the one-level model the

---

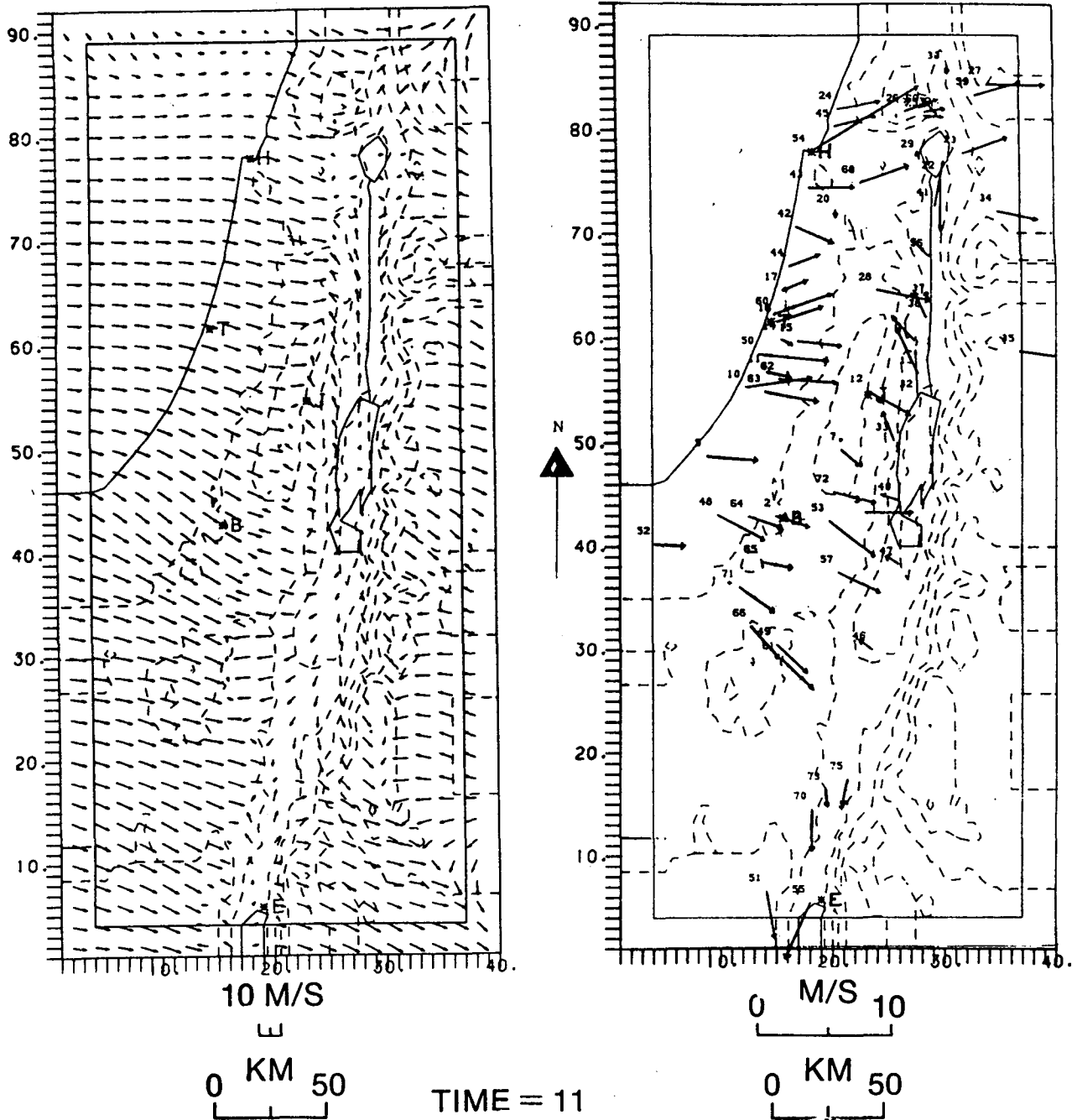[3] For the list of important differences between the models, see Table 1.

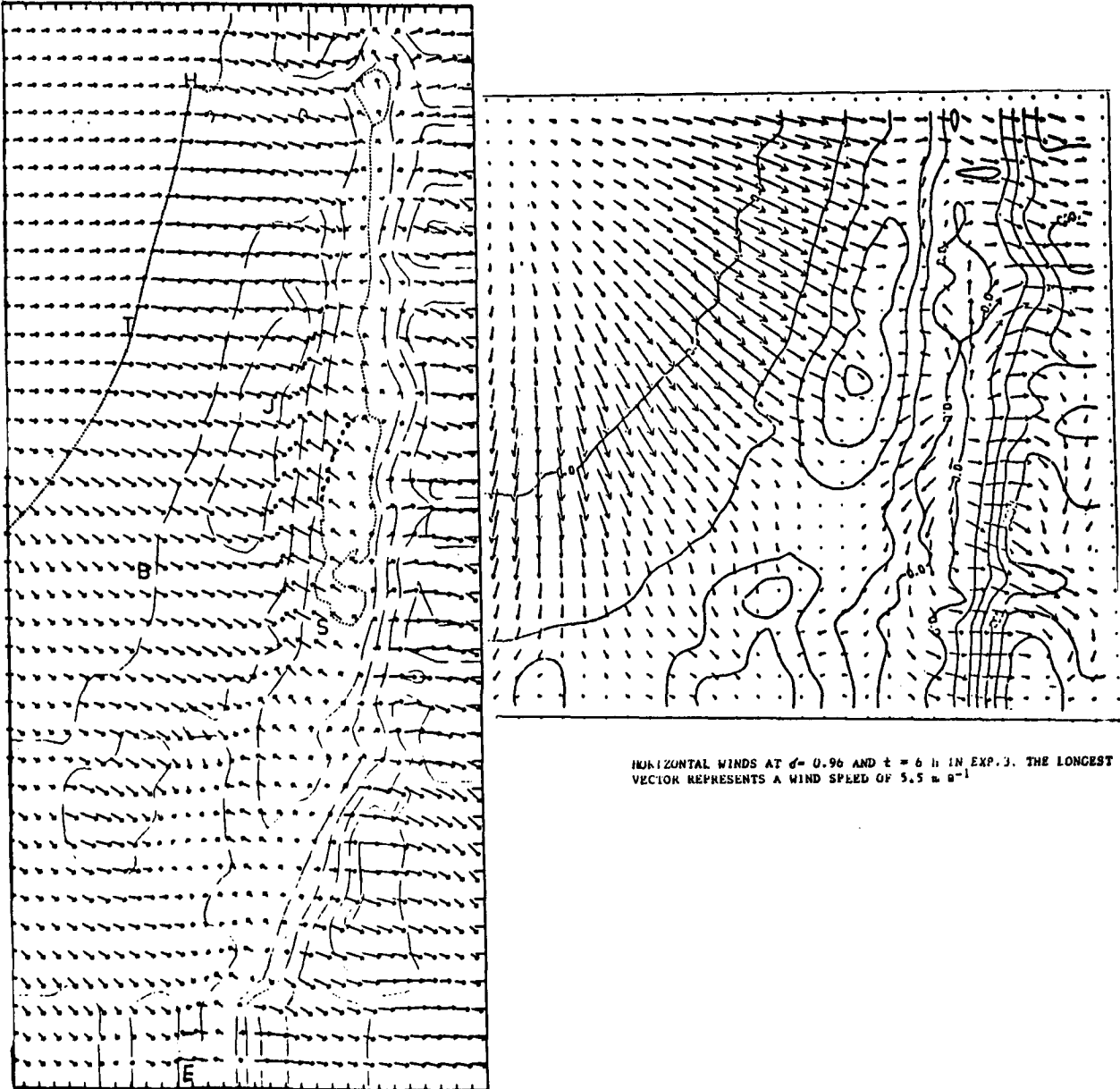FIG. 7. (a, b) As in Fig. 4a; b but for 1100 LST.

eastern boundary is further to the east. For example, in the one-level model the model area extends 50 km east to the Dead Sea while in MS the respective distance is only about 30 km. In the aforementioned regions, i.e., to the east of Galilee and to the northeast of Eilat, this results, for the one-level model, in a distinct topographical upsloping toward the west near the boundary and an enhancing of the eastern anabatic flow. But these easterlies seem to become too strong, particularly in the north, probably due to boundary

effects. The relatively strong northeasterly wind at Eilat was again not reproduced by either model.

(v) *1400 LST:* The prominent feature of the flow at this afternoon hour is the strong Mediterranean sea-breeze winds, which veered clockwise to the north while strengthening in both model simulations and observations. The wind veering between 1100 and 1400 LST is particularly evident at the central coastal plain and in the Northern Negev (compare Figs. 8a–8c to Figs. 7a–7c). In the north, the SBF has penetrated into the

HOUR ⋅ 11.00 LST   10 M/S
HORIZONTAL VELOCITY AT 5.M

HORIZONTAL WINDS AT d= 0.96 AND t = 6 h IN EXP.3. THE LONGEST
VECTOR REPRESENTS A WIND SPEED OF 5.5 m s⁻¹

FIG. 7. (*Continued*) 7(c) As in Fig. 4c but for 1100 LST. (d) The 3-D model results from AW for six heating hours. For the exact time of simulation, see text. The largest vector represents a wind speed of 5.5 m s⁻¹.

Kinneret Valley (Sea of Galilee) and into the north of the JRV both in the models and in the observations. However, this SBF penetration into the JRV and further to the south is clearly retarded in the one-level model simulation (Fig. 8a).[4]

_____

[4] For a full discussion of the breakout of the SBF into Lake Kinneret and its exact timing, see Alpert et al. (1982), which applied a high-resolution, two-dimensional cross-sectional model over northern Israel.

At 1400 LST the aforementioned convergence line in the JRV between the northerlies and the southerlies is located at 1400 LST, 50 to 60 km north of the Dead Sea (between observations sites 36 and 37 in Fig. 8b), while in the 3-D simulation (Fig. 8c), it is only 30 to 35 km north. Although not accurate, location of the convergence line is much better predicted by the 3-D model than by the one-level model, where it stays south of Lake Kinneret. Again, neither model predicts the northerlies at the southern Arava Valley or the vigorous northeasterlies at Eilat.

10 M/S

0 KM 50

TIME = 14
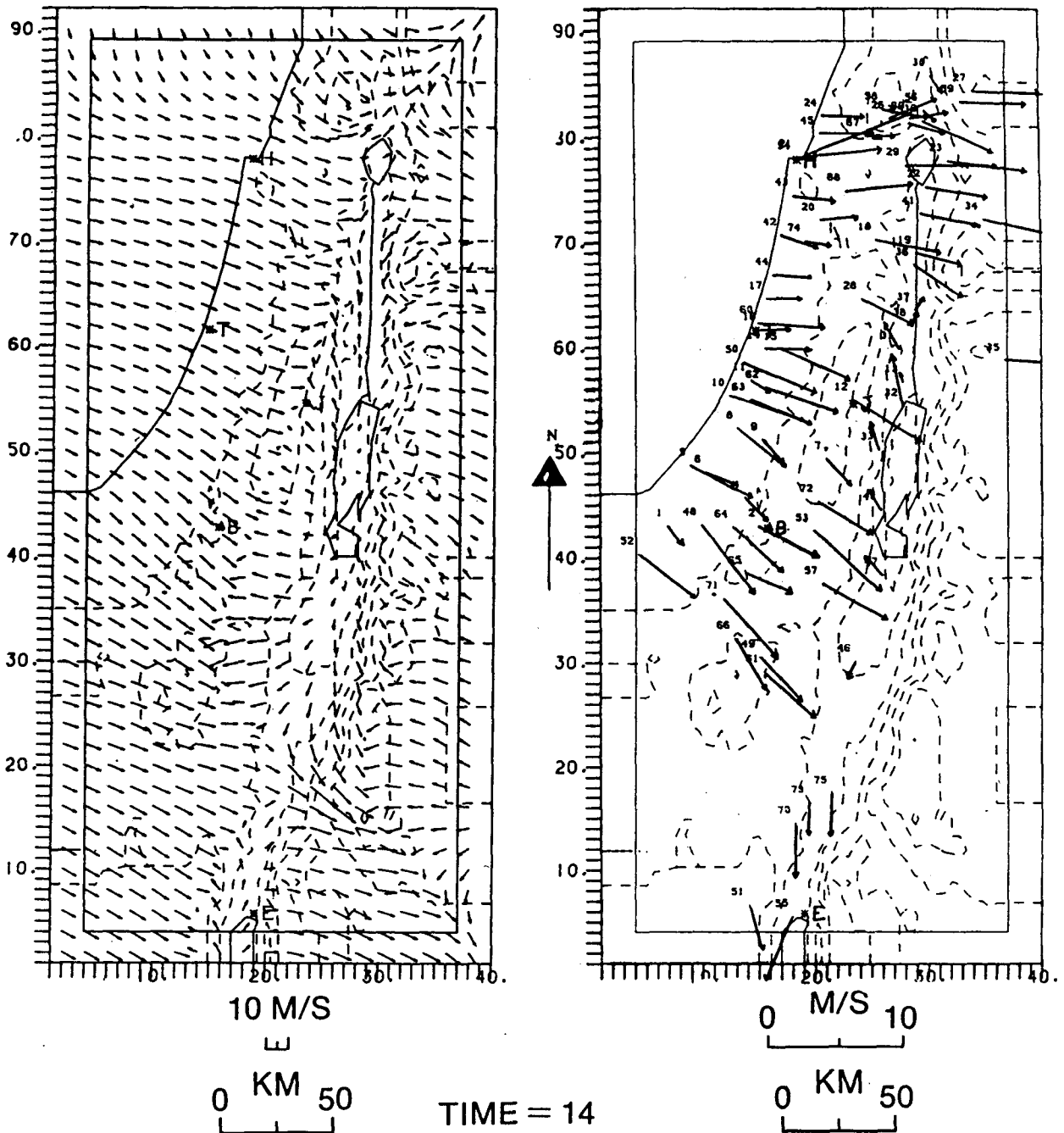
0 M/S 10

0 KM 50

FIG. 8. (a, b) As in Fig. 4a; b but for 1400 LST.

There are several smaller-scale flow features that are indicated by the observations and resolved by the one-layer model but not with the 3-D simulation.

1) At the southeastern slope of the Galilee Mountains, winds turn to the southwest.

2) At the western shore of the Dead Sea winds are south-southeasterly.

3) At the central region of the JRV *southwesterly* winds are observed (stations no. 37 and 38). This flow direction was indicated by Skibin and Hod (1979).

Also, at the southern coast of the Mediterranean, the northwesterlies are stronger and turn toward the north as compared to the winds on the northern coastal plain. This was simulated by the models, but the differences in the wind intensities between the southern and northern coastal plain are not as significant as in the observations.

(vi) *1700 LST:* At this late afternoon hour the SB winds have veered further clockwise toward the north-northwest and strengthened. The SBF has penetrated

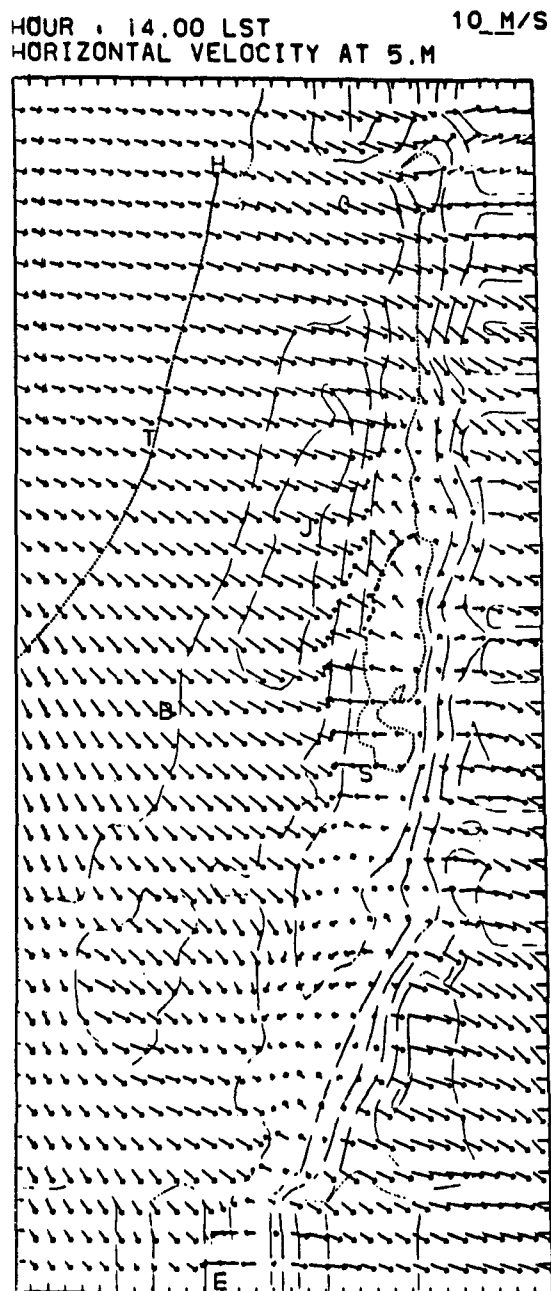HOUR : 14.00 LST   10 M/S
HORIZONTAL VELOCITY AT 5.M

FIG. 8c. As in Fig. 4c but for 1400 LST.

the JRV and reached the western coast of the Dead Sea. An extraordinary feature is the vigorous wind intensities on the lee side of the First Mountain Line (Galilee through the Judean to the central Negev Mountains), which attain *average* values as high as 10 m s^{-1} and abruptly churn the surface of Lake Kinneret stormy, between 1400 and 1500 LST (see Serruya 1978).

At this time the SBF simulated by the one-level model remains at basically the same location, which leaves the lee side of the First Mountain Line still dom-

inated by the southeasterlies (see Fig. 9a) rather than the observed quite strong northwesterly Mediterranean sea-breeze winds (Fig. 9b). The 3-D simulation by MS advances the SBF (Fig. 9c) but not enough. The western coast of the Dead Sea, for instance, is still dominated by the southeasterlies, but in the earlier 3-D simulation S82, the SBF does penetrate the northern section of the Dead Sea (see Fig. 9d). This apparent contradiction between the two simulations by the same group could be explained by a somewhat different input (compare Table 1 in S82 and Fig. 1 in S85). Mahrer and Segal (1984) and S85 ran their model with input values for a specific day which was found to be the closest to the averaged July profiles, while S82 used the actual July averaged profiles (personal communication, Y. Mahrer).

(vii) *2000 LST:* At this time, about an hour past sunset, the winds above the coastal plain of Israel have weakened considerably. But, at the lee side of the mountains, the northwesterly winds are still quite strong and are probably partly enhanced due to the commencement of the katabatic drainage flow into the JRV and the Arava Valley (see Fig. 10b). In the one-level simulation (Fig. 10a) there are weak westerlies above the lee side of the mountains which represent the katabatic contribution. But, they are not strong enough (in the one-level simulation), probably because the daily sea-breeze remnants have not penetrated the lee-side region. This major problem will be further discussed in the next section. However, the sea-breeze remnants at the coastal plain do look quite similar to observations with low speeds of about 1-3 m s^{-1}.

Another feature of the coastal plain flow at this evening time is the higher wind speeds of 2-3 m s^{-1} within 5-6 km of the coast, while further inland but still in the coastal region (8-20 km onshore) winds are consistently weaker, typically less than 1 m s^{-1}. This flow feature can be explained by the quite different roughness over land and sea. Points closer to the Mediterranean Sea attain higher wind speeds comparable to those offshore, while farther inland the higher land roughness diminishes the surface wind intensity. Alestalo and Savijärvi (1985) have investigated through numerical simulations the coastal convergence associated with the differential roughness and concluded that this explains major climatic cloud features near Helsinki, Finland. Following their results the length scale of the coastal convergence cells are on the order of 10 km, and this basically agrees with our results. But their horizontal resolution (Δx = 4 km) and ours (Δx = 5 km) seem to be insufficient for a finer definition of the horizontal scale of the coastal convergence.

On the coastal plain of Israel, there is an additional deceleration of the wind inland by the commencement of the opposing nocturnal katabatic pressure gradient. This reversal in the pressure-gradient force associated with the night flow down the western slopes probably affects even the Mediterranean Sea winds. The models do simulate this coastal speed gradient (see Figs. 10a,
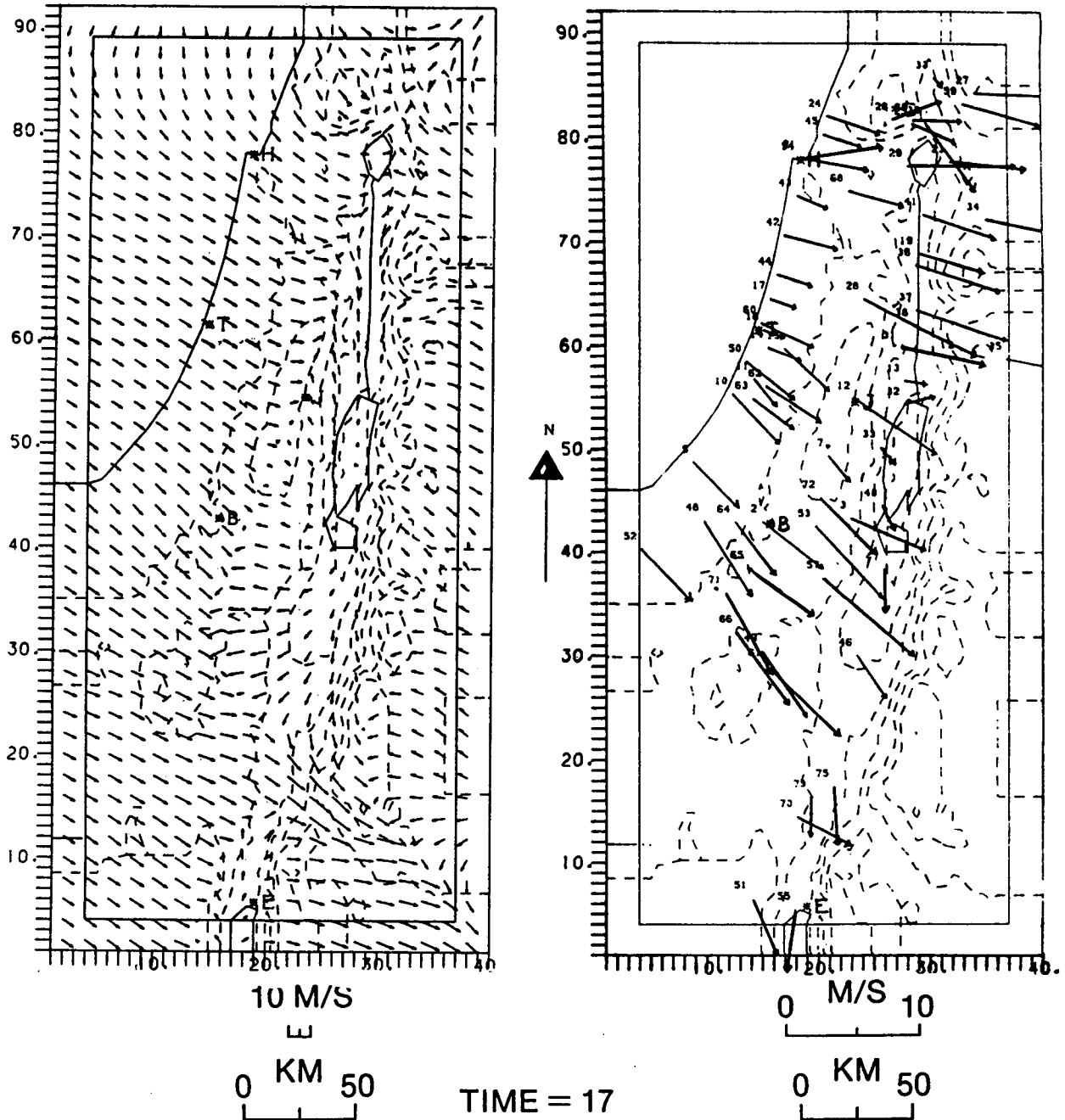
FIG. 9. (a, b) As in Fig. 4a, b but for 1700 LST.

10c), but the sharp gradient is mainly at the coast rather than a few kilometers inland, as evidenced in the observations (Fig. 10b). This discrepancy could be partly explained by the insufficient horizontal resolution in the models. Further investigation, with both models and observations, seems necessary to find whether additional physical (or numerical) factors are involved.

(viii) *2300 LST:* To complete the summerly diurnal cycle that we started at 0200 LST, we now turn to the mesoscale circulation features one hour before midnight (see Figs. 11a, 11b). Unfortunately, we were not

able to find 3-D model simulations for this hour. The basic flow features in the one-level model simulation (Fig. 11a) and in the observations (Fig. 11b) are similar to those at 0200 LST (Figs. 4a–4c) and at 0500 LST (Figs. 5a–5c). Over the Golan Heights, for instance, the flow observations (stations 27 and 39) indicate westerly winds, while the models keep on predicting drainage flow (i.e., easterly winds) into the Kinneret Valley and the Hula Valley to the north. This discrepancy could be the result of the relatively coarse resolution in the models. Further investigation with a much

HOUR , 17.00 LST   10_M/S
HORIZONTAL VELOCITY AT 5.M

HOUR : 1700 LST
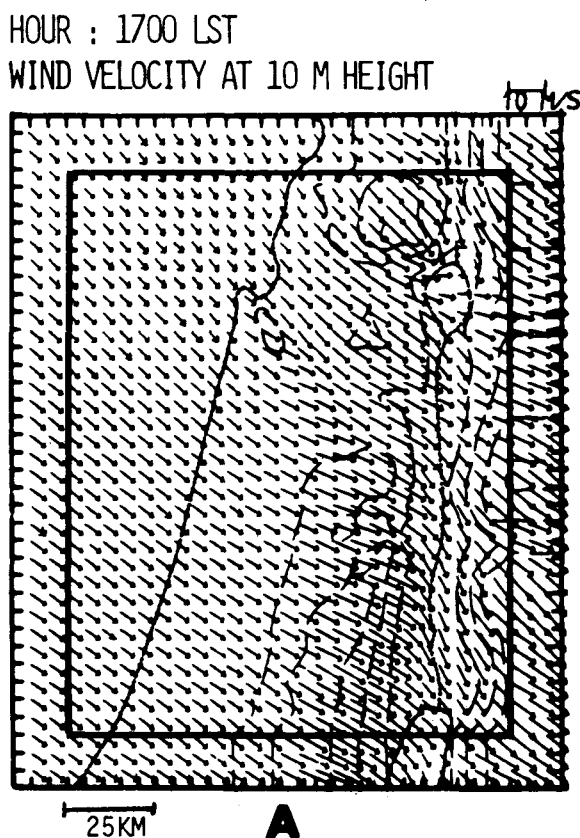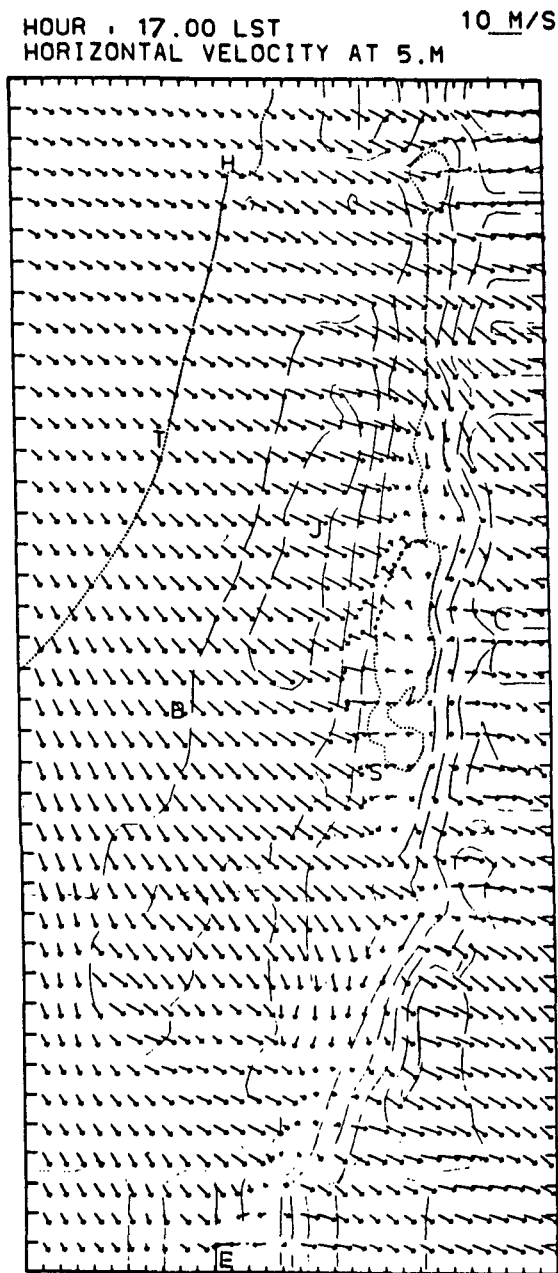WIND VELOCITY AT 10 M HEIGHT

25KM   A

FIG. 9. (Continued) (c) As in Fig. 4c but for 1700 LST. (d) As in Fig. 4c but for 1700 LST and from S82.

higher horizontal resolution is needed to determine the resolution adequate for simulation over such highly variable topography as that of Lake Kinneret and the Golan Heights. Of course, higher resolution might not work if the model does not contain the dynamics that could determine these features at small scales. Another way to determine the appropriate resolution is by studying the spectrum of the topography variance, as suggested by Young et al. (1984).

The night flow down the slopes to the JRV and the Arava Valley is stronger at 2300 LST (Fig. 11b) than later at night at 0200 LST. Further weakening of this

lee-side katabatic flow occurs at 0500 LST (compare Figs. 11b, 4b and 5b corresponding to the hours 2300, 0200 and 0500 LST). In the model, wind intensities and directions correspond well to the observations, but the gradual weakening does not occur. On the contrary, the wind speed slightly increases during the night in some points. We do not know whether this discrepancy is unique to the one-level model or exists in the 3-D simulations as well (since the 3-D simulations were not available at the pertinent hours).

Another interesting feature is the as yet unorganized coastal southerly to southeasterly winds which are the
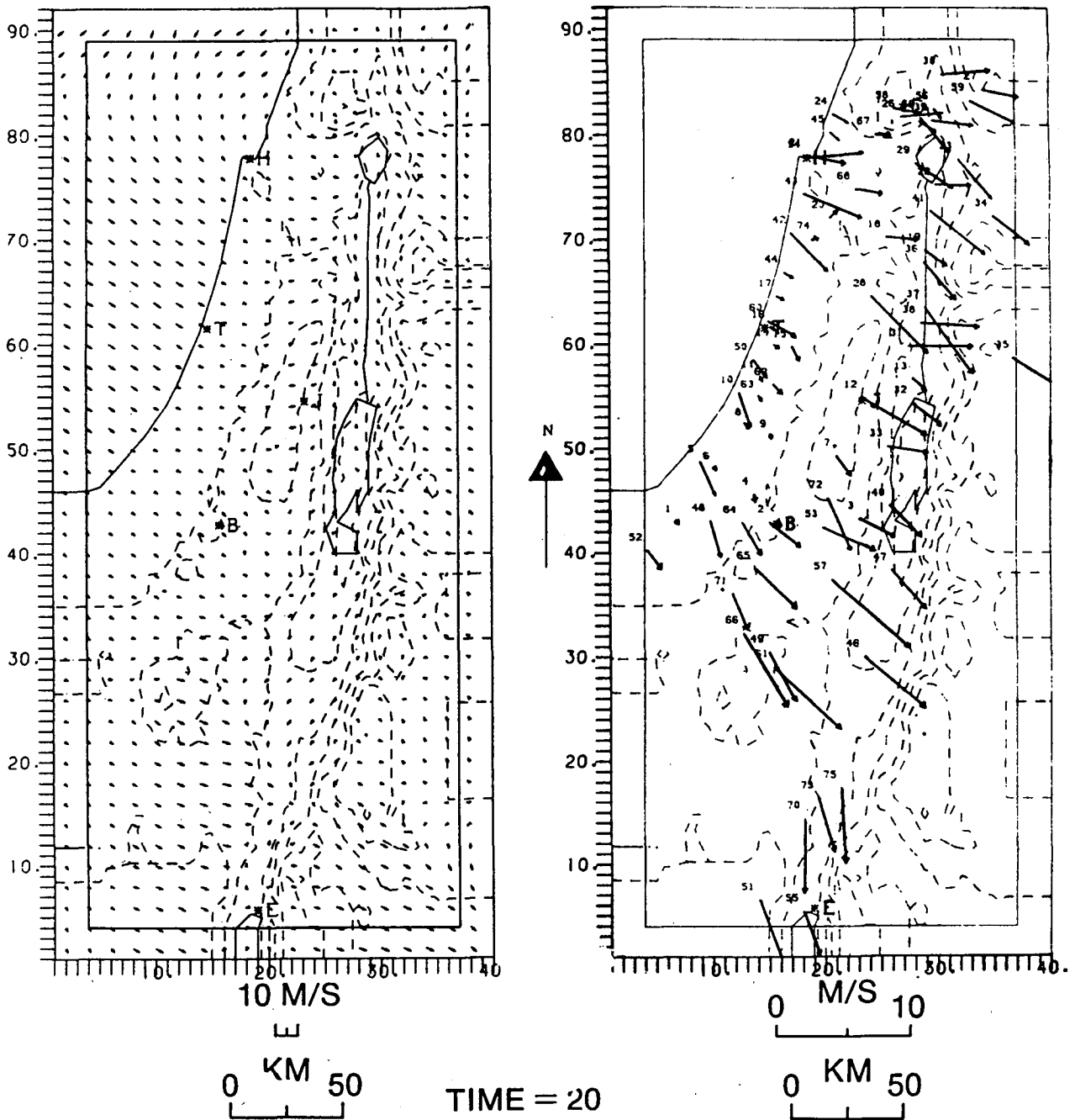
FIG. 10. (a, b) As in Fig. 4a, b but for 2000 LST.

combined result of the land breeze and the katabatic flow. As expected from land-breeze theory, these southeasterly winds gradually strengthen during the night (e.g., see Doron and Neumann 1977), but on the southern coastal plain (20 to 60 km south of Tel Aviv) the winds at this time, although very weak, are still from the west. This might be explained by the gentler slope of the *Southern* Judean Mountains and the Negev Mountains, which diminishes the down-slope contri-

bution to the southeasterly winds on the southern coastal plain. The difference between the two coastal regions also appears in the one-level model simulation (Fig. 11a), where the southeasterlies are weaker in the southern coastal plain.

From the foregoing discussion the following question arises: What is the physical reason for the gradual weakening of the night flow down the eastern slope (toward the Kinneret Valley, JRV and the Arava Val-

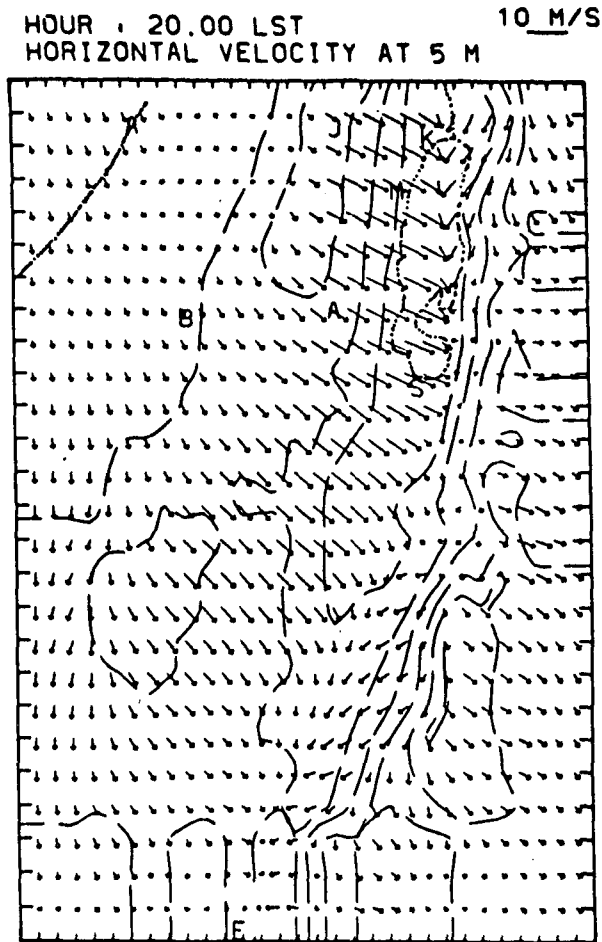HOUR : 20.00 LST   10 M/S
HORIZONTAL VELOCITY AT 5 M

FIG. 10c. As in Fig. 4c but for 2000 LST and from S85.

ley) while the counterpart flow down the western slope (toward the Mediterranean Sea) gradually strengthens from 2300 through 0200 to 0500 LST?

The eastern slope is steeper[5] and the western side slopes toward the Mediterranean Sea, which evidently leads to an additional land-breeze contribution. We may expect this land-breeze contribution on the western slope to increase during the night, but the same does not apply to the eastern slope where land breezes do not exist and the flow evolution is dictated mainly by the katabatic flow. Following the model simulations (see later), we suggest that the reason is to be found in the different initial conditions in the evening over the two slopes. The eastern slope starts the night with the vigorous lee winds (up to ~ 10 m s^{-1}), which are associated with the SBF (e.g., see Figs. 10b, 10c). Hence, the gradual weakening of the wind at night represents primarily the dissipation of these strong winds super-

imposed upon the much weaker slope wind, which develops gradually. The western slope, however, starts the night with weak westerlies, the daily sea-breeze remnants, and the night flow then represents the gradual development of the opposing southeasterly katabatic/land-breeze flow. But the one-level model simulation, which lacks the strong sea-breeze winds on the lee side, shows erroneously that the katabatic flow gradually increases during the night on both slopes. Hence, if the one-layer model was correctly initialized with the stronger evening sea-breeze winds, we might have obtained the observed decreasing trend above the lee side (eastern slope). This was not done here, because the model started at about sunrise and the SBF penetration was not well simulated. But in the cross-sectional study by Alpert et al. (1982), in the northern part of Israel, this decreasing trend on the western shore of Lake Kinneret was well simulated.

4. Conclusions and discussion

The surface-wind fields simulated by the one-level model are very encouraging. The winds for average summer conditions were found comparable to those of 3-D simulations. In some cases, the one-level model was capable of predicting observed flow features that were not simulated by the 3-D simulations, probably due to the finer grid in the one-level model. The one-level model does particularly well at night. It is also encouraging that the deficiencies in the one-level, 2-D and in the 3-D simulations were similar. Most of the discrepancies in the 3-D results were believed to be predominantly (excluding sparse data regions) the result of inadequate resolution over complex topography (e.g., see Segal et al. 1982b, p. 1760). Hence, if higher resolution simulations were carried out, results might be considerably improved. Of course, the model was not yet tested on smaller scale features, i.e., small hills, and the current parametrizations may not be appropriate for such scales. The modest computer resources required by the one-level model enables higher resolution not yet possible with 3-D simulations.

The one-level model was found very useful in the analysis of detailed surface flow, although the model was not successful in correctly advancing the SBF beyond a mountain ridge crest. The SBF remained at essentially the same location along the mountain crest during the afternoon hours. This drawback seems to be common to one-level or one-layer models. Keyser and Anthes (1977) encountered the same problem with their mixed-layer model, although some improvement was later achieved by the modification of the upper boundary condition (Anthes et al. 1982). But as illustrated by Alpert et al. (1982, p. 1004) with a 2-D cross-sectional model, the abrupt penetration of the SBF into the JRV and Lake Kinneret was accompanied by a reversal of the density gradient and the pressure-gradient force at an *upper level*. The existing parametri-

---

[5] The possible contribution of a steeper slope to the features of the katabatic flow may need a separate investigation.
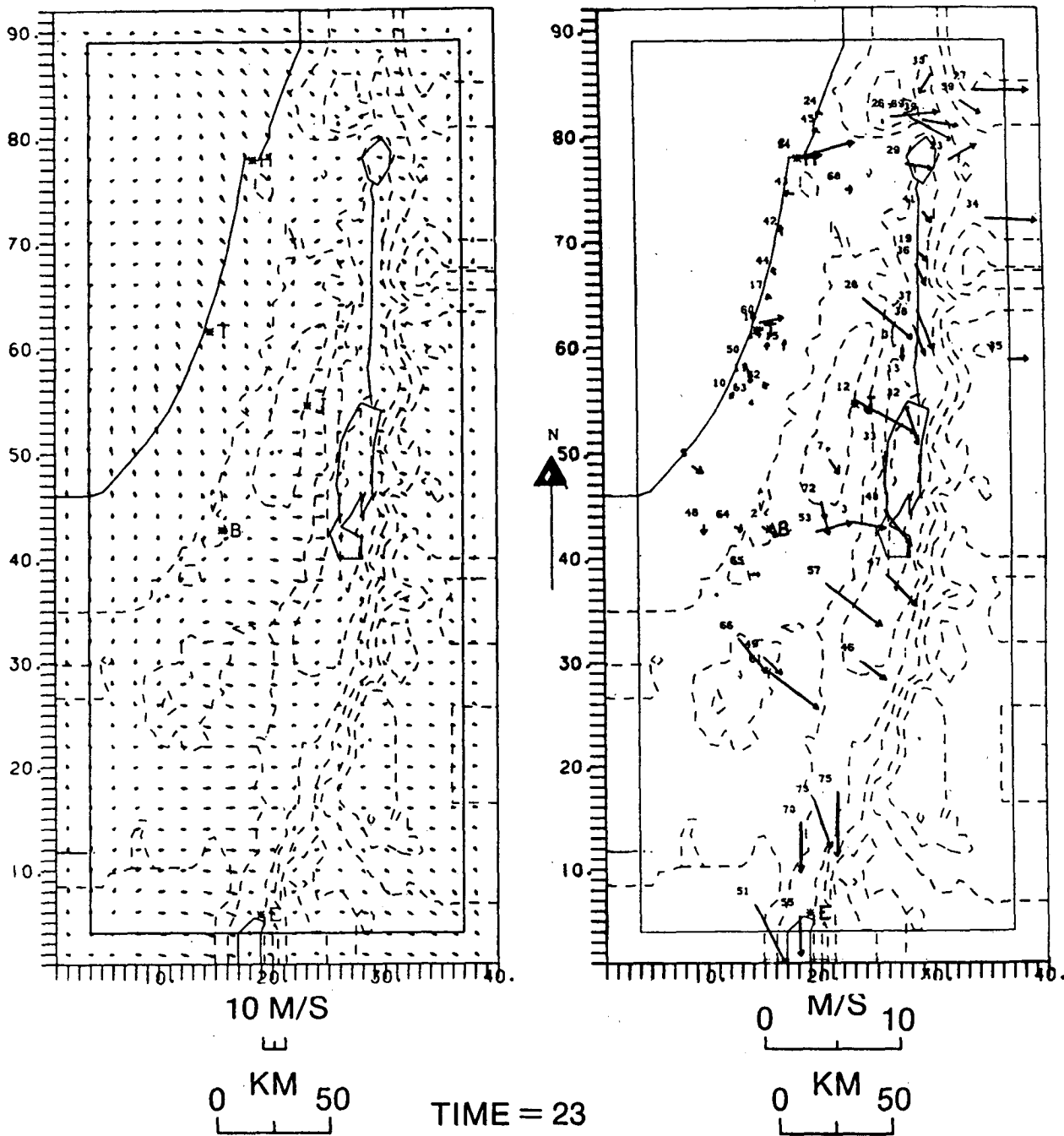
FIG. 11. (a, b) As in Fig. 4a, b but for 2300 LST.

zations in the one-level or one-layer models evidently cannot account for such a mechanism. However, in other respects the results seem to justify application of high resolution, one-level models.

Our observational and modeling study has revealed some mesoscale flow features previously unknown in an area that has been extensively studied in the past. A few examples follow:

(i) Coastal convergence appears in both models and observations at the early evening hour, 2000 LST, and may explain the typical evening line of low stratocumulus clouds along the coast in summer. The counterpart morning line of clouds offshore is also explained by a similar convergence line over the Mediterranean Sea at the early morning hour, 0500 LST. While the latter is over the sea, the former is formed on land and

the physical mechanisms are entirely different. The evening line is the result of the coastal convergence (see Alestalo and Savijärvi 1985), whereas the morning line is formed by the land breeze/katabatic wind which counteracts the large-scale westerly flow offshore (Figs. 5a, 5c).

(ii) Late in the morning, at 1100 LST, a convergence zone in the northern JRV, just a few kilometers south of Lake Kinneret, is formed. This convergence zone penetrates the JRV and moves toward the south, until it unifies with the Mediterranean SBF which penetrates the JRV. At 1400 LST the "front" is at approximately 50 km north to the Dead Sea, and in the evening it reaches the northern shore of the Dead Sea.

(iii) Another interesting feature of the *late* night flow, at 0200 and 0500 LST, is the stronger southeasterlies at the more southern coast, i.e., at 20 to 60 km south of Tel Aviv compared to the southeasterlies north of Tel Aviv. This stronger land breeze/katabatic flow might be explained by the concave shore there.

The aforementioned discoveries illustrate the major advantage of a collaborative high-resolution modeling and observational effort. The special contribution of the one-level model is emphasized. In part II of this study the applicability of the one-level model to real-data forecasting will be investigated.

APPENDIX

List of Symbols

A_1	$1 - (\Gamma/\gamma_2)(1 - C_2)$
A_2	$\Gamma[C_1(\gamma_2^{-1} - \gamma^{-1}) - C_2\gamma_2^{-1}]$
A_3	$\Gamma\gamma^{-1}(T_s/T_R)$
C_1	T_s/T_H
C_2	$T_s \ln C_1/(\gamma_2 H)$
C_D	drag coefficient, section 2b (i)
C_p	specific heat at constant pressure for dry air
e_1	$(T_s\gamma_2^{-1})[T_H^{-1} - (H\gamma_2)^{-1} \ln(T_s/T_H)]$
e_2	T_s/T_H
f	Coriolis parameter
$\mathbf{F}$	frictional force
g	gravitational acceleration
H	depth of "layer of topographic influence"
k	Von Karman's constant
$\mathbf{k}$	unit vector in the vertical
$K_{m,T}$	horizontal turbulent diffusivities for momentum (*m*) and temperature (*T*)
p_s	surface pressure
Q	diabatic heating rate
R	ideal gas constant for dry air
t	time variable
T_H	temperature at height Z_H
T_R	temperature at height Z_R, the reference level
T_s	surface temperature
$\mathbf{V}_s$	(u_s, v_s) surface wind vector
z_0	roughness length
Z_H	$z_s + H$, top of layer of topographic influence
Z_R	height of reference level
z_s	surface elevation
γ	lapse rate between Z_R and Z_H
γ_2	lapse rate within the layer of topographic influence
Γ	g/C_p (the dry adiabatic lapse rate)
σ	p/p_s vertical coordinate

REFERENCES

Alestalo, M., and H. Savijärvi, 1985: Mesoscale circulations in a hydrostatic model: Coastal convergence and orographic lifting. *Tellus*, 37A, 156–162.

Alpert, P., and J. Neumann, 1984: On the enhanced smoothing over topography in some mesometeorological models. *Bound. Layer Meteor.*, 30, 293–312.

——, and A. Eppel, 1985: A proposed index for mesoscale activity. *J. Climate Appl. Meteor.*, 24, 472–480.

——, A. Cohen, J. Neumann and E. Doron, 1982: A model simulation of the summer circulation from the Eastern Mediterranean past Lake Kinneret in the Jordan Valley. *Mon. Wea. Rev.*, 110, 994–1006.

——, A. Eppel and B. Getenio, 1985: Surface wind prediction over complex terrain—application of a one-level terrain following model to Israel. *Seventh Conf. on Numerical Weather Prediction*, Montreal, Amer. Meteor. Soc., 369–373.

——, B. Getenio and R. Rosenthal, 1988: One-level diagnostic modeling of mesoscale surface winds in complex terrain. Part II: Applicability to real-data forecasting. *Mon. Wea. Rev.*, 116, 2047–2061.

Anthes, R. A., and T. T. Warner, 1978: Development of hydrodynamic models suitable for air pollution and other mesometeorological studies. *Mon. Wea. Rev.*, 106, 1045–1078.

——, N. L. Seaman and T. T. Warner, 1980: Comparisons of numerical simulations of the planetary boundary layer by a mixed-layer and multi-level model. *Mon. Wea. Rev.*, 108, 365–376.

——, D. Keyser and J. W. Deardorff, 1982: Further considerations on modelling the sea breeze with a mixed-layer model. *Mon. Wea. Rev.*, 110, 757–765.

Danard, M., 1977: A simple model for mesoscale effects of topography on surface winds. *Mon. Wea. Rev.*, 105, 572–580.

Dickerson, M. H., 1978: MASCON—A mass consistent atmospheric flux model for regions of complex terrain. *J. Appl. Meteor.*, 17, 241–253.

Doron, E., 1979: Objective analysis of mesoscale flow fields—Israel and trajectory calculations. *Israel J. Earth Sci.*, 28, 33–41.

——, and J. Neumann, 1977: Land and mountain breezes with special attention to Israel's Mediterranean coastal plain. *Israel Meteor. Res. Papers*, 1, 109–122.

Goodwin, W. R., G. J. McRae and J. H. Seinfeld, 1979: A comparison of interpolation methods for sparse data: Application to wind and concentration fields. *J. Appl. Meteor.*, 18, 761–771.

Haltiner, G. J., and R. T. Williams, 1980: *Numerical Prediction and Dynamic Meteorology.* 2nd ed., Wiley and Sons, 477 pp.

Haurwitz, B., 1947: Comments on the sea breeze circulation. *J. Meteor.*, 4, 1–8.

Keyser, D., and R. A. Anthes, 1977: The applicability of a mixed-

layer model of the planetary boundary layer to real-data forecasting. *Mon. Wea. Rev.,* **29,** 1351–1371.

Lavoie, R. L., 1972: A mesoscale model of lake-effect storms. *J. Atmos. Sci.,* **29,** 1025–1040.

Mahrer, Y., and M. Segal, 1984: Wind energy simulation with a numerical mesoscale model. Final Rep., Ministry of Energy and Infrastructure, Hakirya, Jerusalem, 27 pp.

——, —— and R. A. Pielke, 1985: Mesoscale modelling of wind energy over nonhomogeneous terrain. *Bound. Layer Meteor.,* **31,** 13–23.

Mass, C. F., and D. P. Dempsey, 1985: A one-level mesoscale model for diagnosing surface winds in mountainous and coastal regions. *Mon. Wea. Rev.,* **113,** 1211–1227.

Neumann, J., 1951: Land breezes and nocturnal thunderstorms. *J. Meteor.,* **8,** 60–67.

——, and Y. Mahrer, 1971: A theoretical study of the land and sea breeze circulation. *J. Atmos. Sci.,* **28,** 532–542.

——, and ——, 1974: A theoretical study of the sea and land breezes of circular islands. *J. Atmos. Sci.,* **31,** 2027–2039.

Segal, M., Y. Mahrer and R. A. Pielke, 1982a: Numerical study of wind energy characteristics over heterogenous terrain—central Israel case study. *Bound. Layer Meteor.,* **22,** 373–392.

——, —— and ——, 1982b: Application of a numerical mesoscale model for the evaluation of seasonal persistent regional climatological patterns. *J. Appl. Meteor.,* **21,** 1754–1762.

——, ——, —— and R. C. Kessler, 1985: Model evaluation of the summer daytime induced flows over Southern Israel. *Israel J. Earth Sci.,* **34,** 39–46.

Serruya, C., 1978: *Lake Kinneret.* Dr. W. Junk Publishers, 501 pp.

Skibin, D., and A. Hod, 1979: Subjective analysis of mesoscale flow patterns in northern Israel. *J. Appl. Meteor.,* **19,** 329–338.

Young, G. S., R. A. Pielke and R. C. Kessler, 1984: A comparison of the terrain height variance spectra of the Front Range with that of a hypothetical mountain. *J. Atmos. Sci.,* **41,** 1249–1250.